Engineering and Technology Journal
Journal homepage: https://etj.uotechnology.edu.iq

A Modified Global Management Controller for a Grid-connected PV System with Battery under Various Power Balance Modes

Diana S. Obaid[a]*, **Ali J. Mahdi**[b], **Mohammed H. Alkafaji**[a]

[a] Electrical Engineering Dept, University of Technology-Iraq, Alsina'a Street, 10066 Baghdad, Iraq.
[b] Electrical Engineering Dept, University of Kerbala, Karbala, Iraq.
*Corresponding author Email: eee.19.38@grad.uotechnology.edu.iq

HIGHLIGHTS

- A microgrid control system that depends on two stages was proposed.
- The battery current and DC-link voltage control systems perform admirably, particularly during mode transitions.
- Positive results with seamless transitions between modes were obtained from simulations conducted for various solar panels, battery status, and grid power.

ARTICLE INFO

Handling editor: Ivan A. Hashim

Keywords:
Photovoltaic system; energy management system; energy storage system; DC-DC bidirectional converter; droop control.

ABSTRACT

This work presents an Energy Management System (EMS) constructed on dissimilar power balance modes and dynamic grid power to activate a DC-link microgrid with a solar (PV-array) generator and battery storage. In addition, the option of requesting adjustable power from the grid to encounter load demand is also presented. Based on the availability of solar sources, battery state, and grid power, energy management offers the appropriate references for all modes. Six power balance options are defined based on power supply, storage system, and grid mobility to match the load requirement. The aims are to reduce energy usage and upsurge the life of the storage device. The microgrid is controlled to maintain a consistent DC-link voltage and manage the battery current depending on the mode of operation. Using MATLAB\SIMULINK software, the anticipated energy management system, which is based on power balancing modes, is tested under various scenarios. The simulation results demonstrated that the microgrid operated admirably, with seamless switching between power balance modes.

1. Introduction

Smart microgrids and small-scale founded on renewable energy sources have converted popular in the previous decade. Microgrids harvest about 4 GW of energy globally, with North America accounting for 67 percent of total power production [1]. A small-scale microgrid, conscience, and ecologically friendly electricity grid that uses dispersed renewable energy sources. It has the facility to function in both islanded and grid-connected modes. The microgrid also could track in parallel with the main utility grid, rejecting the need for high dispersion. Microgrids also seek economic profits, high-efficiency networks, power distribution, and long-term energy backup, among other things [1,2]. The microgrid could be made from a single or series of interconnected units. The generating, control and communication units are the main apparatuses of a microgrid, where the best consumption of dispersed energy sources (DER) can result in economic and environmental assistance [3,4]. The microgrid might be DC-link, AC-link, or hybrid contingent on the point of common coupling (PCC). DC microgrids have continually been preferred for small-scale generation over solar (PV), and a battery storage system (BSS**)** can be suddenly connected to the DC-link as a power electronic converter with the smallest amount of complication [5,6]. Dissimilar layers of control and local controllers for the units of generating, as well as the system of energy management, are contemporary in a microgrid system (EMS). Supervisory control and data acquisition (SCADA) is a term used to describe the EMS as a top-level control [5-9].

Several pieces of research have been published in the microgrid control field and EMS [8-19]. As a result, the EMS can be implemented with certain improvements with real-time simulation for efficient management, enhanced microgrid-based

http://doi.org/10.30684/etj.2022.132323.1102
Received 26 November 2021; Accepted 21 April 2022; Available online 24 September 2022
2412-0758/University of Technology-Iraq, Baghdad, Iraq

controlling on the fuzzy-logic system (FLS), or dealing with the energy of microgrid setups with efficient optimization methods like particle swarm optimization (PSO).

The works [20-22] provided optimal energy management under uncertain conditions. Prioritization in these works was given to battery life and size, efficiency, and price compensation in the EMS. In [1], the experimental/hardware application of the EMS, while considering the dynamic grid price, battery states, and intermittent renewable generation, is a serious difficulty in microgrid operation to solve the difficulties of the EMS algorithm.

To solve the disadvantages of integrating the EMS algorithm into the control system, this research proposes an Economic management system (EMC) that depends on the generated power and the BSS to provide the load demand and sell the surplus power to the main grid. Only when the battery and PV cannot cover the load will the grid require intervention to contribute supply power load—the EMS with numerous modes for competently operating the microgrid in various scenarios. The purpose of this research is to look into the power balance in a medium-scale simulation microgrid in various scenarios. The importance of coordinated BSS with the grid is proven in this work through real-world scenarios. The difference between this work and the others is the use of programming code to control the operation of BSS on EMS. Another important aspect of the current work is the creation of a rule-based EMS system that uses different power balance modes to ensure optimal operation while taking into account battery condition, PV generation, grid power, load demand, mitigation of transient issues, and introducing smart EMS using a global algorithm, which is used as a control to the local control system for each unit.

This paper is organized as follows: Section 2 describes the microgrid configuration and the dynamics of its components. Then, in section 3, the PV-array configuration explains the local control units for the PV (mppt). Then, section 4 explained the system controller. Finally, section 5 focuses on the proposed energy management system, where all the operating conditions are considered to provide the reference current for the battery storage system.

2. Proposed Microgrid Configuration

The proposed configuration of a microgrid is composed of a PV system connected to the DC link by a directional uni-directional boost converter, a battery storage system connected to a bi-directional buck-boost converter to keep the system stable under various modes, a two-level inverter connected to the LC filter, variable load for the test system and it is connected at PCC. The whole system is connected to the main grid by an interface transformer, as demonstrated in Figure 1.

The power of the PV system and battery system are provided by Equations (1 &2) as follows:

$$P_{pv} = V_{pv}\, I_{pv} \tag{1}$$

$$P_{bat} = V_{bat}\, I_{bat} \tag{2}$$

The voltage-current characteristics of the battery system can be expressed by:

$$V_{bat} = V_0 - k\,\frac{Q}{Q - \int I_{bat}\, dt} + A.\, e^{(-B \int I_{bat}\, dt)} - R_b I_{bat} \tag{3}$$

where, R_b is the internal resistance of the battery, B is the exponential area time constant inverse, A is an exponential area amplitude, and $\int I_{bat}\, dt$ is the capacity of the battery. To control the charge and discharge of the battery storage system, the calculation of the state of charge is required, and it can be depicted in Equation (4).

$$SOC(t) = SOC(t-1) - \frac{\int I_{bat}\, dt}{Q} \tag{4}$$

For keeping the battery life cycle, the constraint of SOC should be taken into consideration, and it can be demonstrated by:

$$SOC_{min} \leq SOC \leq SOC_{max} \tag{5}$$

Where the SOC_{min} and SOC_{max} minimum and maximum permissible limit depend on battery properties. The active and reactive power of inverter output in dq theory with assuming $\_(d) = V, v\_(q) = 0$, the final expression of active and reactive output power are provided by:

$$P = 3 v_d i_d \tag{6}$$

$$Q = 3 v_d i_q \tag{7}$$

where the, v_d and v_q are the output voltage of inverter in dq theory, and i_d and i_q are the output currents of the inverter in dq theory. It can be noticed from Equations (6 and 7) that the active and reactive power can be controlled by i_d and i_q Respectively.

In grid-connected mode, the power balance for covering load demand is carried out by:

$$P_g = P_L - \left(P_{pv} + P_{bat}\right) - P_{Losses} \tag{8}$$

Where, P_g *and* P_L are the grid and load power, respectively. While P_{Losses} is the power loss in the LC filter. Equation (8) depends on the power management algorithm for supervisory the whole system and keeping the system in balance mode.

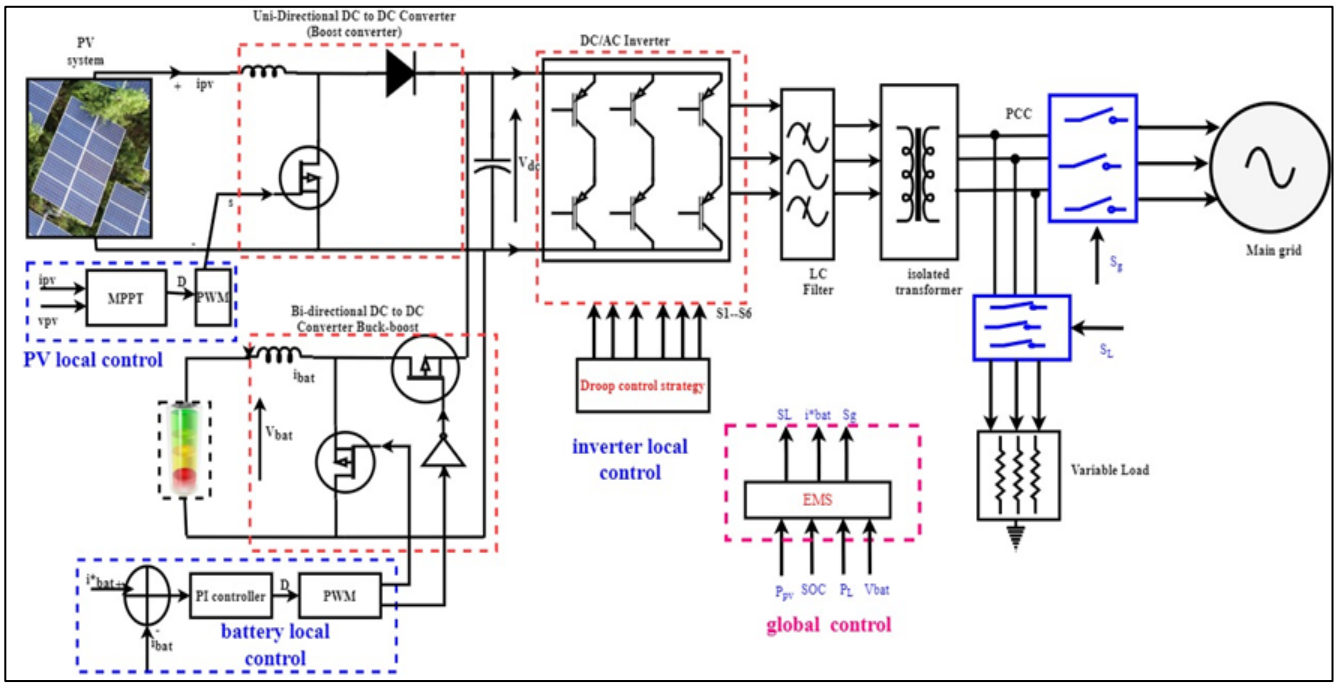

Figure 1: Proposed Microgrid configuration [1]

3. Pv Generator

A linear power source was used to model the PV generator in terms of ambient temperature and irradiance level [8,23]. The total generator's output power at the maximum power point (MPP) is calculated using (9) and (10), where parameters are taken from manufacturer data sheets (nominal operating cell temperature (NOCT) and standard test condition (STC)) [24].

$$P_{pv} = \left[P_{pv,STC} \times \frac{G_T}{1000} \times \left[1 - \gamma \times \left(T_j - 25\right)\right]\right] \times N_s \times N_P \quad (9)$$

where $P_{pv}, P_{pv,STC}, G_T, \gamma, T_j, N_s$ *and* N_P represent the output power of the generator, the power temperature coefficient and the rated PV power at MPP, and STC, the irradiance level at STC, the cell temperature, and the number of modules in series and parallel that made up the generator, respectively. The temperature of the cell is calculated using equation (10), and the NOCT measurement conditions are $T_{amb,NOCT} = 20\,{}^{\circ}{}_C$.

$$T_j = T_{amb} + \frac{G_T}{1000} \times (NOCT - 20) \quad (10)$$

In this paper, the solar power plant is composed of 11 panels in series and 46 panels in parallel to produce a total power equal to 200Kw, and each panel has a 400 w, which includes 90 cells.

4. Control System

This paper focused on how to avoid the islanding issue when the hybrid Renewable energy system RES is disconnected from the main grid due to many reasons such as fault, drop in grid voltage, and grid frequency to keep the hybrid system in stable situations. To solve this problem, the DC to AC side needs for robustness control strategy to present the drop in AC voltage and maintain the frequency operation within the nominal limit. In this study, the droop control is very useful for synchronization between the RES and main grid special in islanding mode. The proposed droop control is depicted in Figure 2. It is composed of three main blocks: power calculation block, droop loop block, and two inner loops block for voltage and current [25, 26]. These blocks are explained in the below sections:

4.1 Droop Control P-F And Q-V

To produce the reference voltage and reference frequency [26], the relationship between P-F and Q-V are calculated by Equations (12 and13) as:

$$f = f^* - m\Delta P \quad (12)$$

$$v = v^* - n\Delta Q \tag{13}$$

The droop coefficients can be calculated as:

$$m = \frac{\Delta\omega_{max}}{P_{nom}} \tag{14}$$

Figure 2 shows the proposed block diagram of the droop inverter that consists of the following blocks: power calculation, droop controller, and inner loops for current and voltage controllers.

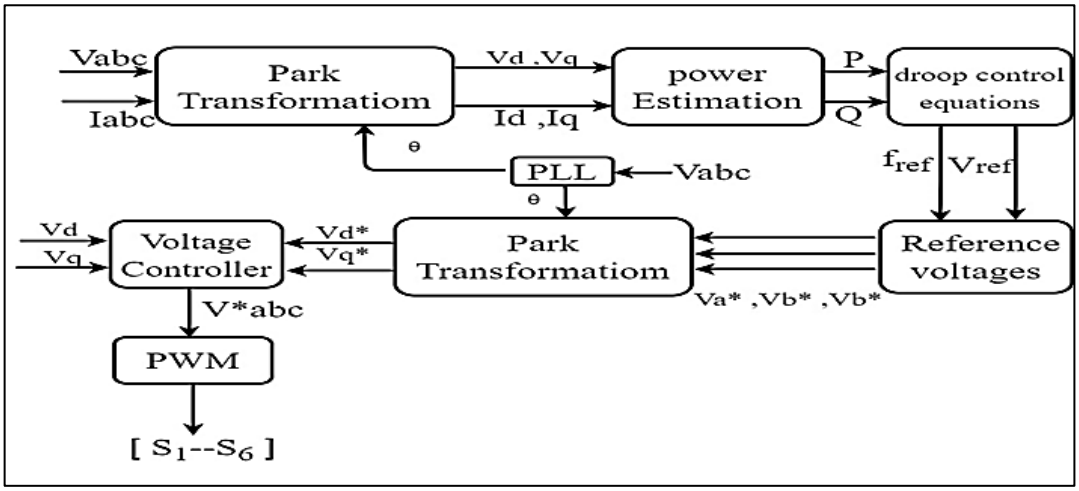

Figure 2: The proposed droop control system [26]

$$n = \frac{\Delta v_{max}}{Q_{nom}} \tag{15}$$

Where f^* and v^* are the nominal frequency of grid voltage and the rated magnitude of phase voltage,$\Delta P = P - P^*$ is a change of active power, $\Delta Q = Q - Q^*$ is the change of reactive power in droop control, m and n represent the coefficients of P-F and Q-V droop control.

Therefore, the three-phase reference voltages can be calculated depending on the output voltage and frequency in the above equation as:

$$v_a = V_{Max}\, sin\, sin\,(wt) \quad v_b = V_{Max} sin\,(wt - 120) \quad v_c = V_{Max}\, sin\,(wt + 120)\,\} \tag{16}$$

4.2 Two Inner Loops

This section presents the internal control loops of voltage and current feedback. The two PI controllers are used to control the actual voltage at the PCC point, as shown in Figure 3. The voltage loop depends on comparing the reference voltage produced by the droop control loop and the actual voltage that is feedback from the PCC point. The output of the PI controller is currents, which are compared with the actual current measured from the PCC point. Finally, the reference generator current is compared with PWM to pluses the six switches of the inverter [24,26].

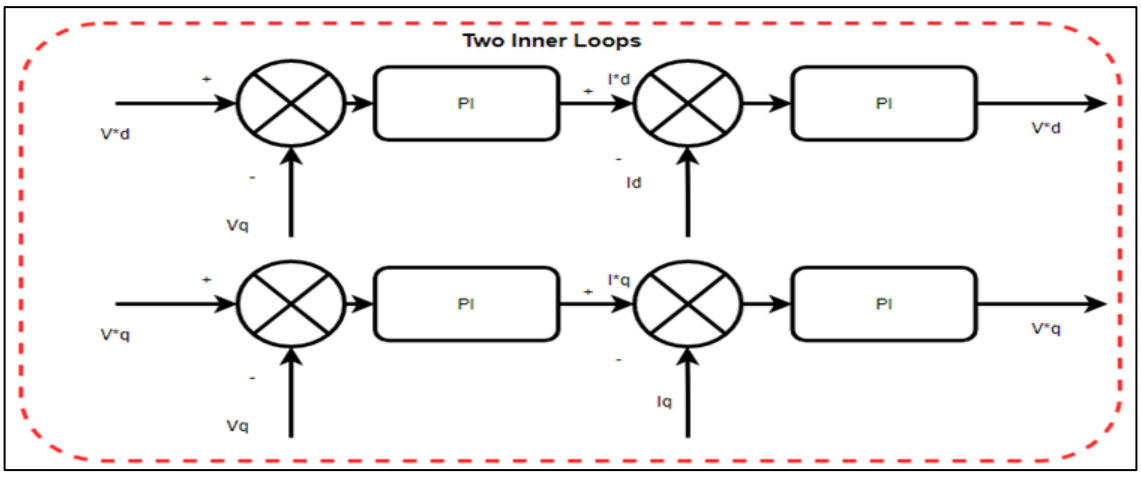

Figure 3: The structure of the two inner loops [26]

5. Proposed Energy Management Algorithm

Herein, the EMS illustrates six modes of the power balance to regulate the power flow and keep the system stable when the load demand suddenly increases (disturbance). Depending on the SOC of the BSS, the availability of the generation power and the availability of the grid of these six modes are shown in Figure 4.

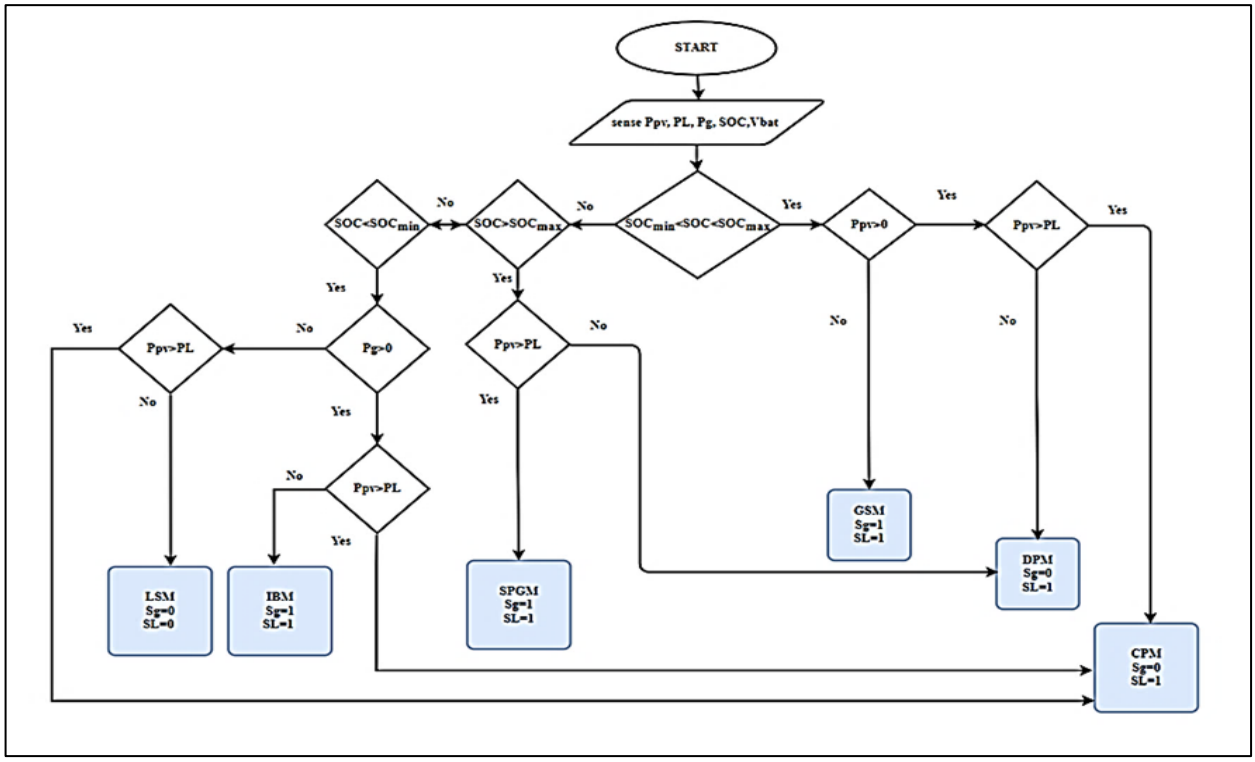

Figure 4: The algorithm of the modified global energy management

The meanings of the symbols presented in the modified global management controllers are as follows: P_g is the main grid power P_L is the load power I^*_{bat} is the current of the BSS, (DPM) is the Deficit Power Mode, (GSM) is the Suitable Grid Mode, and (SPGM)is the Surplus Power Grid Mode. (IBM) is the Idle Battery Mode, (LSM) is the Load shedding mode, and (CPM) is the Charging Power Mode [1]. These modes are explained in the below section as follows:

5.1 GSM

If PV array power is very small (approximately near zero), the load demand is encountered by the BSS and the grid if the BSS's SOC of the battery is in the range [SOC_{min} , SOC_{max}]. In this case, the battery's contribution to the grid is to supply a load for a lengthy period to avoid deep discharge of BSS. The current reference of a battery is given by:

$$I^*_{bat} = \frac{P_L}{V_{bat}} ,\{SOC_{min} \leq SOC \leq SOC_{max}\ P_g > 0;\ P_{pv} \approx 0\ \} \quad (17)$$

5.2 DPM

this mode occurs when the output power of the PV system is less than the demand load. In this case, the battery is contributed with a PV system to supply the demand load without needing the main grid to provide power to the load. Therefore, the current battery reference can be expressed as:

$$I^*_{bat} = \frac{P_{pv}-P_L}{V_{bat}} ,\{SOC_{min} \leq SOC \leq SOC_{max}\ P_L > P_{pv}\ \} \quad (18)$$

5.3 CPM

In this mode, the main grid is unavailable, the output power of the PV system is greater than the demand load, and the battery is not fully charged. In this regard, the PV system and supplying power to the load, and the battery is charged until it reaches maximum SOC. Therefore, the current reference for the battery is provided by:

$$I^*_{bat} = \frac{P_L-P_{pv}}{V_{bat}} ,\{SOC < SOC_{min}\ P_L < P_{pv}\ P_g \approx 0\ \} \quad (19)$$

5.4 SPGM

In this mode, the output power of the PV system is greater than the demand load. In this regard, the battery must be in a maximum SOC, then the PV system supplies the power to the load and sells the remaining power to the grid. The current reference of battery is provided by:

$$I^*_{bat} = 0, \{SOC_{min} \leq SOC \leq SOC_{max} \ P_L < P_{pv} \ \} \quad (20)$$

5.5 IBM

It is a communal scenario in PV array and BSS-based grid-tied inverters anywhere the battery be disposed to deep charge or deep discharge resulting from extreme or lacking DC-side power. Generally, any EMS must consider the battery limits associated with the SOC for safety reasons. If the SOC of the battery is less than the minimum edge, the battery is still deputy or idle, and no power is provided to the load. The load demand will be supplied from the PV array or both the PV array and the main grid. The battery reference current in this scenario is:

$$I^*_{bat} = 0, \{SOC < SOC_{min} \ P_g > 0 \} \quad (21)$$

5.6 LSM

This circumstance indicates that electricity from the grid is unavailable, and the SOC is less than the minimum limit, considering that the PV output power is less than the demand load. For power balance, PV must provide the load demand, and load shedding is essential. In this mode, the PV array delivers the power generated to the important loads according to the priority. The current reference for the battery is written as:

$$I^*_{bat} = 0, \{SOC < SOC_{min} \ P_g \approx 0 \ P_L > P_{pv} \} \quad (22)$$

The flowchart in Figure 4 depicts the EMS's power balance modes in detail. The energy-flow management algorithm controls the active power flow from and to BSS according to the priority of the load supplying depending on available generated power from the PV array, the battery SOC, and the availability of the grid. In case of a sudden increase in demand and a generated power that is unable to cover, the battery storage system interferes with delivering the demand after checking its SOC. SOC will sense all over the operation, and the EMS checks it to keep the battery in charge, we have to define the minimum and maximum limit of SOC for controlling the charge and discharge, and the mode of the system depends on this procedure. If the PV generator and battery fail to deliver power demand, the system checks the grid availability to do this, or the system operates in Saving power mode.

6. Simulation Results

Six modes are considered in this section to demonstrate the effectiveness of the proposed control strategy and the coordination between local and global management control. These modes are divided into two scenarios which are SOC_{min} < SOC< SOC_{max} and SOC<SOC_{min}. The parameters of the PV panel used in this paper are listed in Table 1. The total power generated by the solar power plant to provide the demand load is 200kW. MATLAB software was used to conduct all simulation studies. The simulation results of each scenario are discussed in Table 2 below.

The frequency of the load is a system crucial parameter, and any deviation will lead to a loss of synchronization between PV and grid sides. The frequency deviation can be calculated as Equation 23:

$$\text{Frequency Deviation (FD)\%} = \left(\frac{Nominal\ Frequency - (Maximum\ or\ Minimum\ Frequency)}{Nominal\ Frequency}\right) * 100\% \quad (23)$$

Table 1: Specifications of the proposed PV generator system

Description	Symbol	Value	Unit
Max PowerPoint	MPP	400	W
Open circuit Voltage	V_{OC}	85.3	V
Short circuit current	I_{SC}	5.87	A
Current, at the maximum power point	I_{mpp}	5.49	A
The voltage at the maximum power point	V_{mpp}	72.9	V
Number of parallel panels	N_p	46	-
Number of series panels	N_s	11	-
Total power of solar power plant	P_{total}	200	kW

Table 2: The calculated parameters of the proposed system in Figure 1

Parameters	Value	Parameters	Value
Rated power	200 kW	Boost capacitor	2.2 mF
Grid voltage (L-L)	400 V	Boost inductance	0.67 mH
Grid frequency	50 Hz	DC-link capacitor	7 mF
DC-Voltage	800 V	Filter capacitor	40 µF
Switching frequency	6 kHz	Filter inductance	81.47 mH
Bi-directional inductance	0.3 mH		

6.1 Test 1

Three modes (GSM, DPM, and CPM) are examined to ensure a stable load demand. The GSM is conducted in low solar irradiation throughout the time t=0 sec to t=1 sec, as indicated in Figure 9. The load power is assisted by the battery and the grid, as the PV power is very low, according to the power responses shown in Figure 9. Furthermore, to remain the battery in discharge for a long time, the grid pays for power contributed with BSS, as shown in Figure 8 for GSM. Figure 9 can be seen from this Figure, and its excellent tracking capabilities and no overshoot. Also, as established in Figure 5, the DC-link voltage is well regulated and rejects disturbances during the switch between modes. As seen in Figure 8, the SOC drops from 72 percent to 71.993% during the battery discharge. The PV power is promoted to the high irradiance at t =1.1 sec, and the microgrid is inclined to zero-power from the grid simultaneously. When the power of the PV array is less than the demand loads at t =1.1 sec, the system switches to DPM, which enhances the battery's power involvement to encounter the load demand relative to the prior model. It is obvious from this Figure that the EMS algorithm is a seamless transition between modes, and the voltage of the DC-link is still effectively controlled. A slight transition is observed in all results at (t =1.1 sec.) due to changes in the mode and the PV-array power. Because of the increased power of the PV- array and becoming the PV output generating power is higher than the demand loads. The EMS algorithm is a transition to the CPM. Figures 6, 7, and 9 show that the grid power is almost nil. Furthermore, as shown in Figure 9, the battery declines at a faster rate during CPM operation to charge until it reaches maximum SOC. Finally, the controller follows the procedure that indicates in Figure 4.

The output waveforms of PCC voltages and currents, load current and voltage, and grid current and voltage are shown in Figures (10. a and b), (11. a and b), and (12. a and b), respectively. These figures show that the proposed control algorithm is investigating the synchronizing the PV system voltage with the main grid voltage and that the currents and voltages are pure sine waves that are completely unchanged by sudden weather changes.

The frequency of this test is always stable with allowable limits for all changes, as shown in Figure 13. Table 3 illustrates the min. and max. frequency deviation during the disturbance.

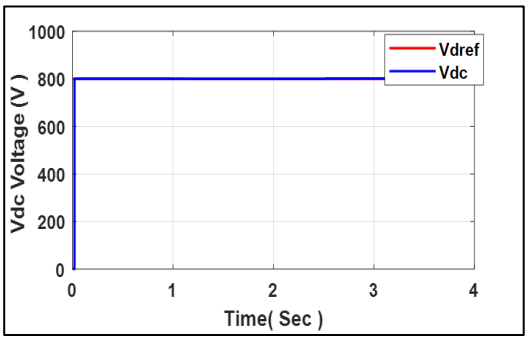

Figure 5: response of DC-link voltage

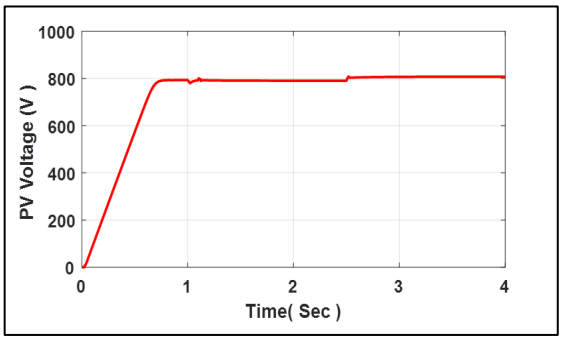

Figure 6: response of PV voltage

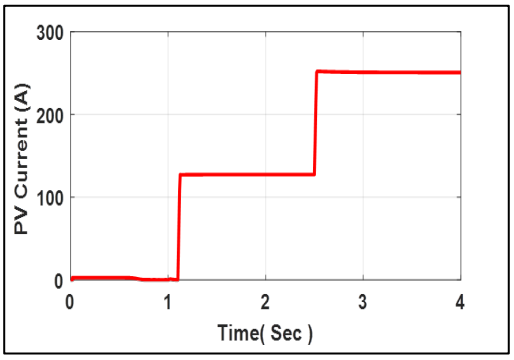

Figure 7: Response to PV's current

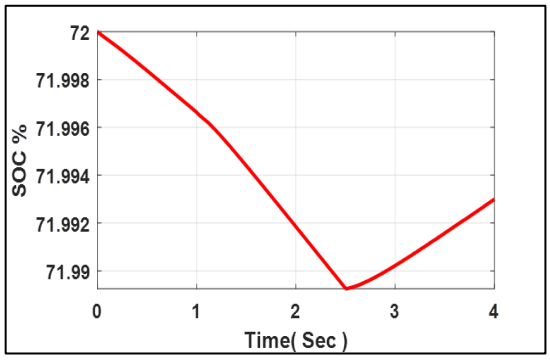

Figure 8: Battery state of charge

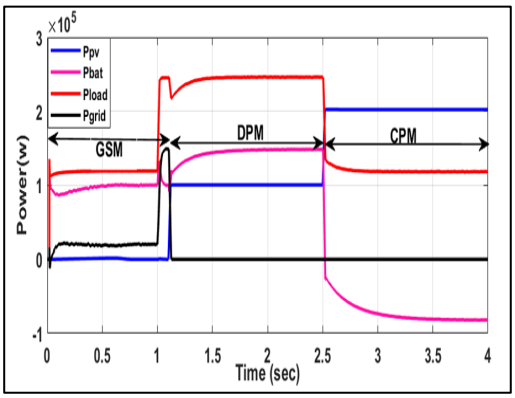

Figure 9: Power flow of proposed system based on EMS algorithm

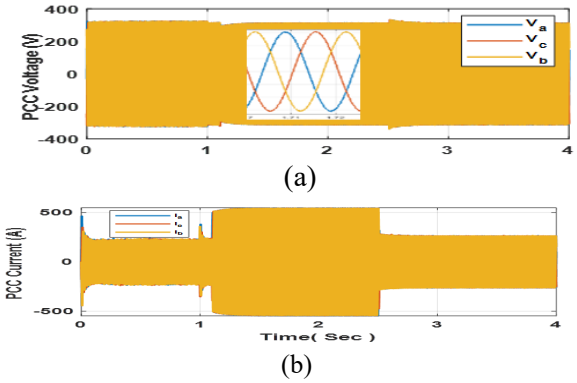

Figure 10: Output waveforms of the inverter at PCC (a)inverter voltage,(b) inverter current

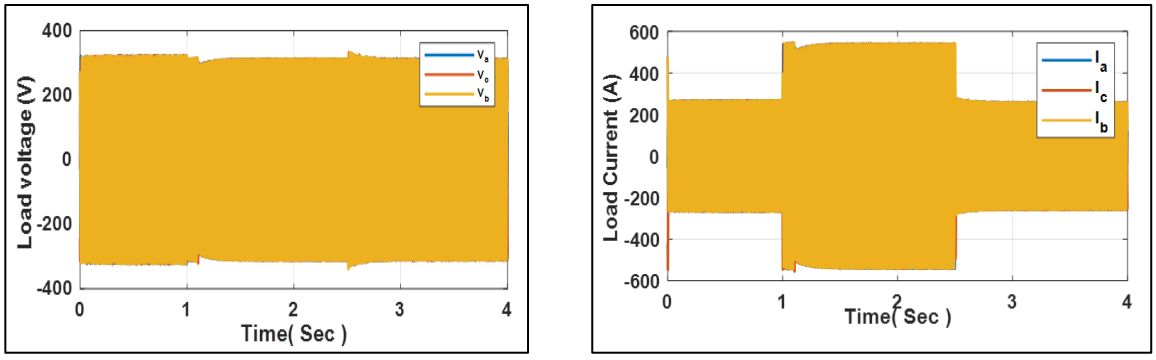

(a) (b)

Figure 11: Load waveforms (a) Load voltage, (b) Load current

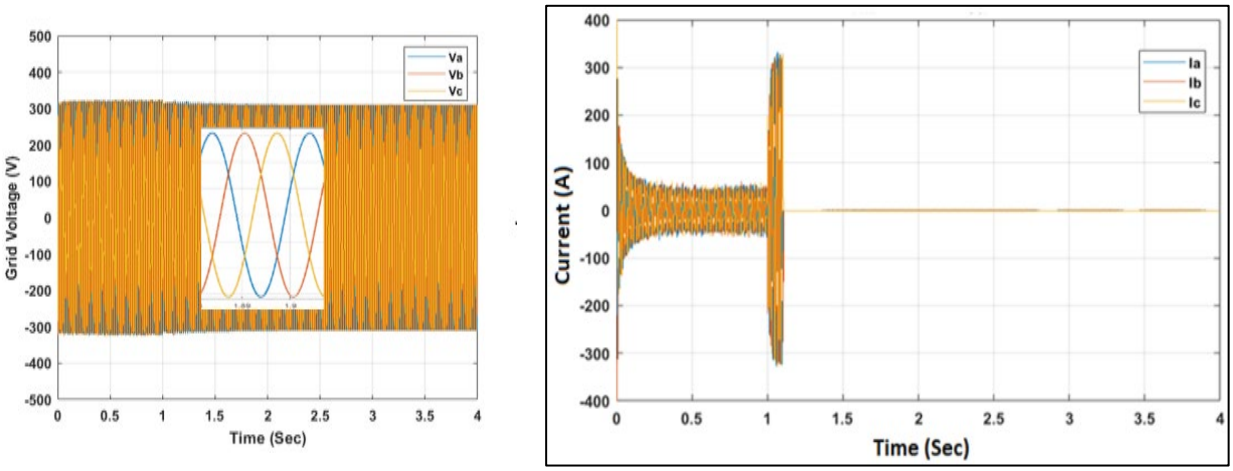

(a) (b)

Figure 12: Output grid waveforms (a) Grid voltage, (b) Grid current

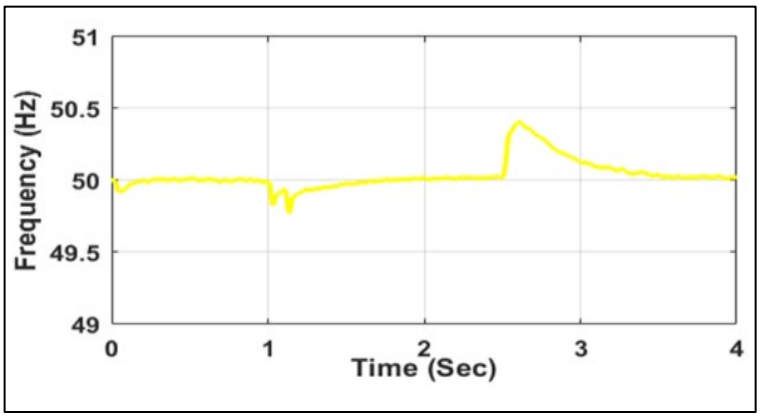

Figure 13: System frequency waveform of test 1

Table 3: Frequency deviation of test 1

Time (s)	Frequency Deviation FD%	State
0.066	0.16	Without disturbance
1.033	0.34	
1.142	0.44	Disturbance in both PV generation and load
2.600	-0.82	

6.2 Test 2

The test includes two modes that occur when the battery is less than the lower limit of charging SOC<20%**.** As demonstrated in Figures 17 and 18, when SOC is less than SOC_{min}, the battery current drops to zero, and the battery's power delivery is nil, as illustrated in Figure (18). To sustain the power balance, the grid and PV deliver power to the load if the load power is greater than the PV power in this mode called IBM. In case load power is less than PV power, the PV supplies the demand power and charges the BSS until it reaches full charge. This mode is called CPM. At each mode, the DC-link voltage, PV current, and PV voltage are shown in Figures 14, 15, and 16. According to the MPPT, the PV voltage is 800 V, and the PV current is practically stretched to 250 A at 1000 w/m^2, which is the rated current. With the changes in the SOC, there is a minor shift in the PV voltage. Regardless of power changes, the DC-link voltage remains constant at 800 V; nevertheless, there is some overshoot at the times t =1 sec and t =2.5 sec. Figure 21 represents the current injection in the grid. The grid three-phase currents fluctuate in response to variations in the generation unit; however, the current direction is determined by the network's power balance mode.

The grid-side current changes at t = 1,1.5 sec, as the operational modes are changing at that moment. Figures 19b, 20.b, and 21.b show PCC's currents, load currents, and grid currents, respectively. The three-phase voltages in the load are always constant and independent of other variables. It can be seen from these Figures; the waveforms have a pure sine wave with some overshoot during the switch between modes and quickly return to the nominal value. Finally, Figures 19.a, 20.a, and 21.a demonstrates the output waveforms of PCC voltages, load voltages, and grid voltages, respectively. These Figures indicate that the proposed control algorithm is investigating the synchronizing between the PV system and the main grid. As in test 1, the system frequency of this test is always stable with allowable limits for all changes, as shown in Figure 22. Table 4, illustrates the min. and max. frequency deviation for this test during the different types of disturbances.

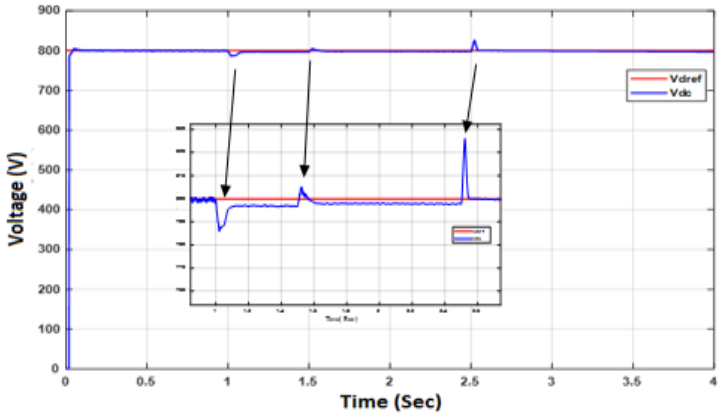

Figure 14: Response of DC-link voltage

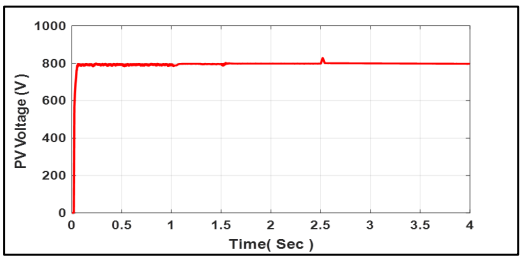

Figure 15: Response of PV voltage

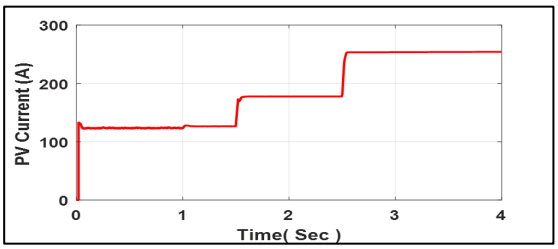

Figure 16: Response of PV current

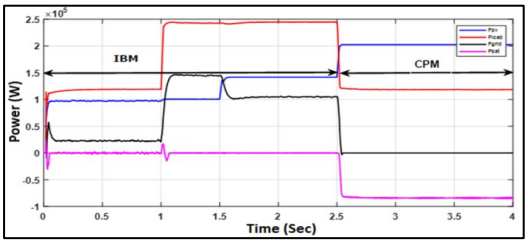

Figure 17: Power flow of proposed system based on EMS algorithm

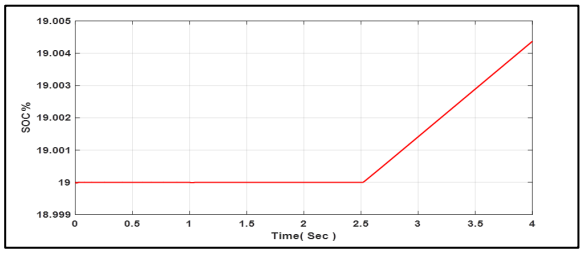

Figure 18: Battery state of charge

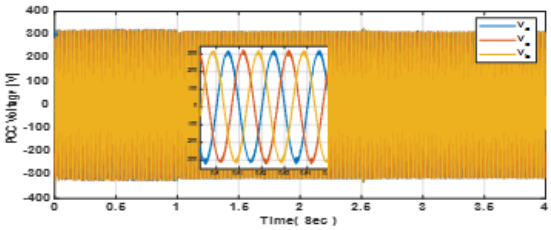

(a)

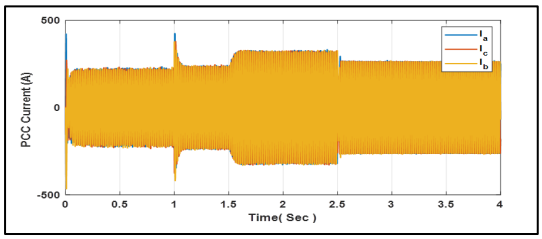

(b)

Figure 19: Output waveforms of the inverter at PCC (a) Inverter voltage, (b) Inverter current

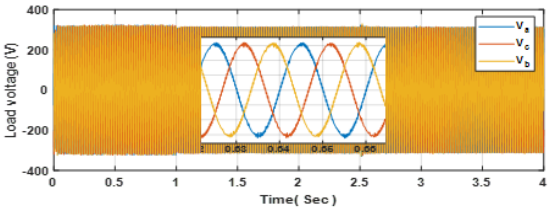

(a)

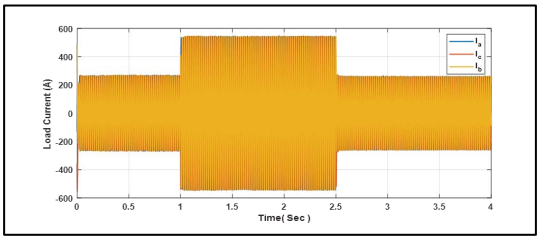

(b)

Figure 20: Load waveforms (a) Load voltage, (b) Load current

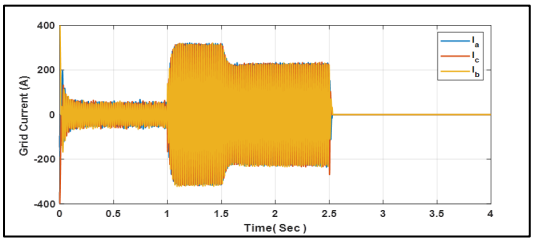

(a)

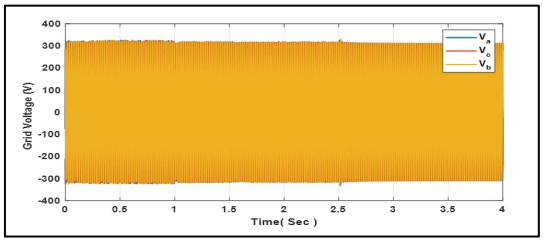

(b)

Figure 21: Output grid waveforms (a) grid voltage, (b) grid current

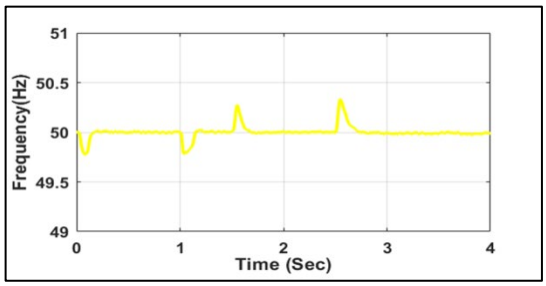

Figure 22: System frequency waveform of test 2

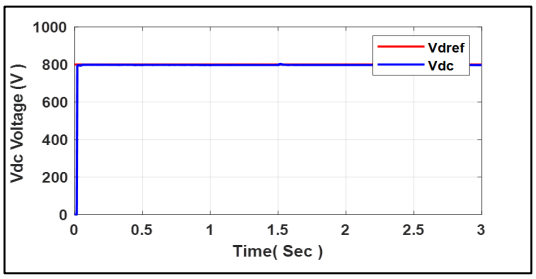

Figure 23: Response of DC-link voltage

Table 4: Frequency Deviation of Test 2

Time (s)	Frequency Deviation FD%	state
0.0749	0.44	Without disturbance
1.0380	0.44	
1.5570	-0.54	Disturbance in both PV generation and load
2.543	-0.64	

6.3 Test 3

This test explains two system modes that occur when the grid is disconnected because of islanding or any disturbance on the grid side and when the SOC of the BSS is less than the lower limits shown in Figures 26 and 27. The battery current dropped to zero, and no battery power was delivered to the load, so power demand was supplied from the PV array only. At the time =0, when the load is greater than the source capacity, we have to switch off unnecessary loads in this mode called LSM. At time =1.5 sec, the demand is less than the power generation from the PV. The power is delivered to the load and, simultaneously, charges the battery in this mode called CPM. At each mode, the DC-link voltage, PV current, and PV voltage are shown in Figures 23, 24, and 25. According to the MPPT, the PV voltage is 800V, and the PV current is practically stretched to 250A at 1000 w/m^2, which is the rated current. With changes in the SOC, there is a minor shift in the PV voltage. Regardless of power changes, the DC-link voltage remains constant at 800V; nevertheless, at the times t =1.5 sec.

Figures 28.b, 29.b, and 30.b show PCC's currents, load currents, and grid currents, respectively. The three-phase voltages in the load are always constant and independent of other variables. It can be seen from these Figures; the waveforms have a pure sine wave with some overshoot during the switch between modes and quickly return to the nominal value. Finally, Figures 28.a, 29.a, and 30.a demonstrates the output waveforms of PCC voltages, load voltages, and grid voltages, respectively. These Figures indicate that the proposed control algorithm is investigating the synchronizing between the PV system and the main grid.

As for tests 1 and 2, the system frequency is always stable with allowable limits for all changes, as shown in Figure 31. Table 5 illustrates the min. and max. frequency deviation for this test during the different types of disturbances.

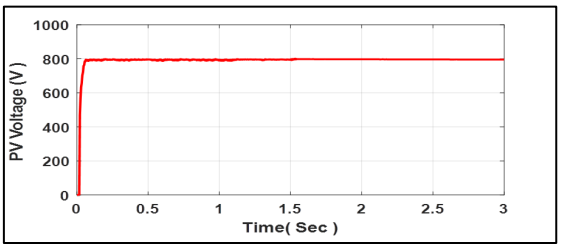

Figure 24: Response of PV voltage

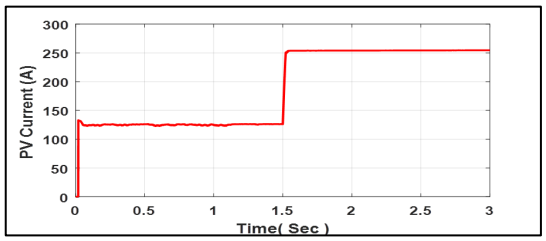

Figure 25: Response of PV current

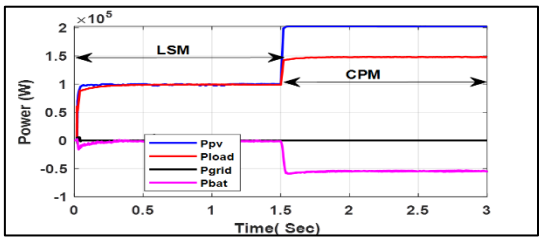

Figure 26: Power flow of proposed system based on EMS algorithm

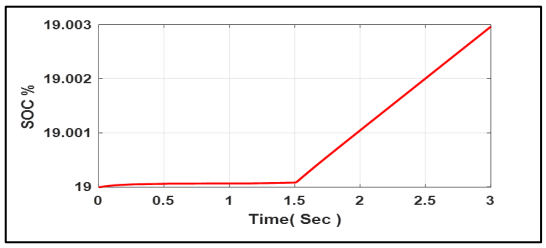

Figure 27: Battery state of charge

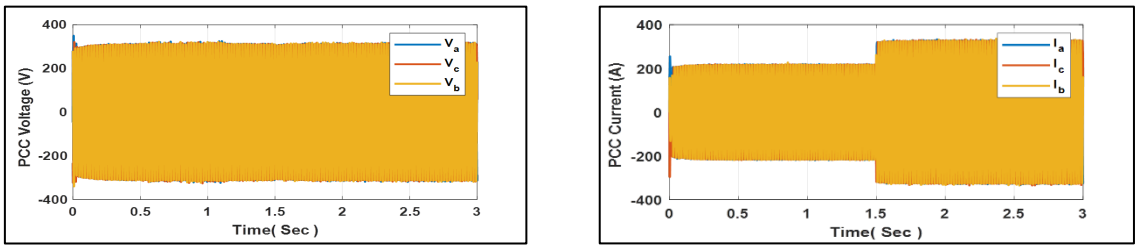

(a) (b)

Figure 28: Output waveforms of the inverter at PCC (a) inverter voltage, (b) inverter current

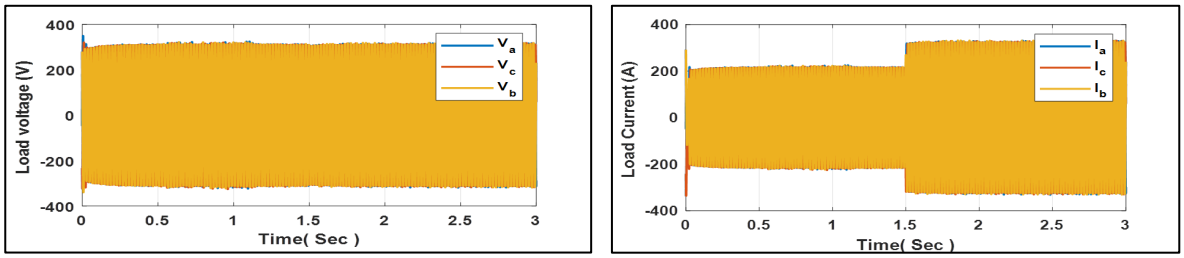

(a) (b)

Figure 29: Load waveforms (a) load voltage, (b)load current

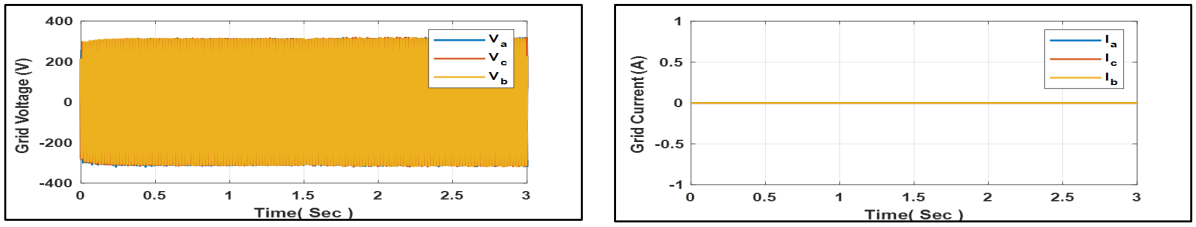

(a) (b)

Figure 30: Output grid waveforms (a) grid voltage, (b) grid current

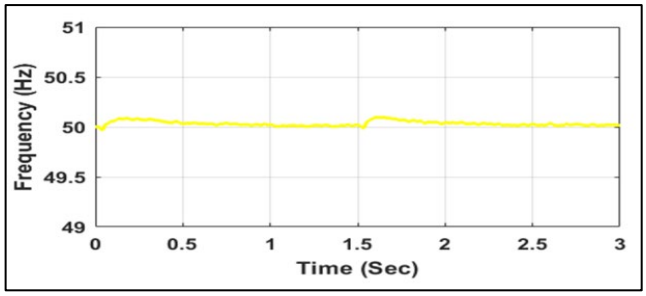

Figure 31: System frequency waveform of test 3

Table 5: Frequency deviation of test 3

Time (s)	Frequency Deviation FD%	State
0.039	0.06	Without disturbance
0.1854	-0.18	
1.5350	0.02	Disturbance in both PV generation and load
1.6140	-0.20	

6.4 Test 4

This test explains that the system's two modes occur when the grid is available and when the SOC of the BSS is greater than the upper limits. At t=0 sec. the load power is less than the generated power, the battery current drop to zero, and no battery power is delivered to the load. Hence, power demand is supplied from the PV array only, and the surplus power sold to

the grid(SPGM) occurs. At the time =2 sec, when the load is greater than the source capacity, the battery contributes with PV-array to supply the power to the load (DPM) occur this power management is shown in Figure 32.

It should be noted that this paper is compared with Reference [1]. to present the extent of the improvement as summarized in Table 6.

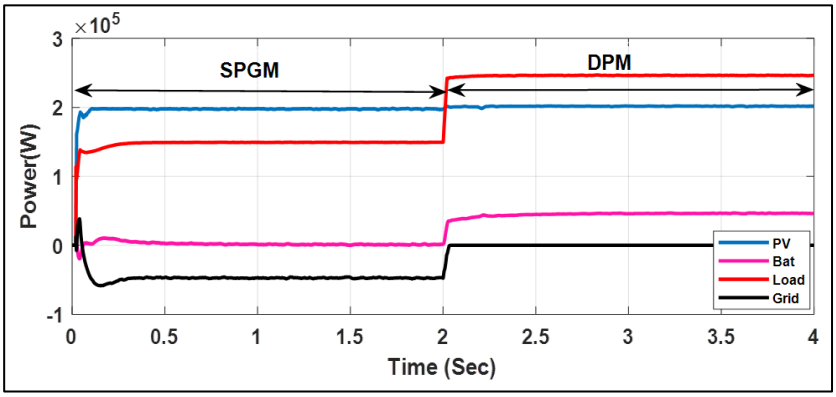

Figure 32: System Power management waveform of test 4

Table 6: A comparison between the current work and Dhar et al. work [1]

Item	Reference [1]	This Paper
PV Generation rating	Small-scale 86.9 W	Medium-scale(100-200) kW
Load rating	Constant approximately 140 W	Variable (150-250) kW
Factors considered in the proposed algorithm	Price of the grid power	SOC of the BSS
Control technique	fuzzy logic system based on the grid price (as the input) and the optimization factor (as the output).	Embedded MATLAB algorithm for coordination between the PWM controllers of the PV generator and the BSS
Methodology	Demonstrating the cost analysis of a microgrid	Applying the Droop controller to stabilize the grid frequency under various disturbances
DC link performance	Not discussed	Investigated
Topology of power filter	RL	LC

7. Conclusion

This paper proposes a microgrid control system that depends on two stages: local control to govern the DC link and get the maximum power from the PV system and global control, which is the EMS algorithm to make a balance between the generation side and load side. The EMS algorithm has seven power balance modes, with self-power generation and grid power transfer choices. The battery current and DC-link voltage control systems are performing admirably, particularly during mode transitions. Simulations were conducted for various solar panels, battery states, and grid power, and the results were positive, with seamless transitions between modes. To find the best values for present references, future work could include using artificial intelligence tools like nature-inspired optimization algorithms. Furthermore, integrating prediction algorithms for solar irradiance and load demand for load preparation and reducing a cost function related to energy pricing and gas releases can improve the energy management system.

Author contribution

All authors contributed equally to this work.

Funding

This research received no specific grant from any funding agency in the public, commercial, or not-for-profit sectors.

Data availability statement

The data that support the findings of this study are available on request from the corresponding author.

Conflicts of interest

The authors declare that there is no conflict of interest.

References

[1] R. K. Dhar, A. Merabet, A. Al-Durra , A. M. Y. M. Ghias, Power Balance Modes And Dynamic Grid Power Flow In Solar Pv And Battery Storage Experimental Dc-Link Microgrid, IEEE Trans. Power Syst. Access, 8 (2020) 219847-219858. https://doi.org/10.1109/access.2020.3042536

[2] M. Zolfaghari, S. H. Hosseinian, S. H. Fathi, M. Abedi And G. B. Gharehpetian, A New Power Management Scheme For Parallel-Connected Pv Systems In Microgrids, IEEE Trans. Sustainable Energy, 9 (2018) 1605-1617. https://doi.org/10.1109/tste.2018.2799972

[3] G. V. Somanath Reddy, V. P. Mini, N. Mayadevi And R. Hari Kumar, Optimal Energy Sharing In Smart Dc Microgrid Cluster, 2020 IEEE International Conference on Power Electronics, Smart Grid and Renewable Energy (PESGRE2020), Cochin, India, 2020, 1-6. https://doi.org/10.1109/pesgre45664.2020.9070405

[4] A. Wahid. Et Al. A Novel Power Scheduling Mechanism for Islanded Dc Microgrid Cluster, Sustainability, 12 (2020) 6918. https://doi.org/org/10.3390/su12176918

[5] T. Abderrahim, And B. Said, Control And Management Of Grid Connected Pv-Battery Hybrid System Based On Three-Level DCI, 2017 6th International Conference on Systems and Control (ICSC), Batna, Algeria, 2017, 439-444. https://doi.org/10.1109/icosc.2017.7958709

[6] B. N. Alhasnawi, B. H, Jasim, P. Siano, J. M. Guerrero, A Novel Real-Time Electricity Scheduling For Home Energy Management System Using The Internet Of Energy, Energies, 14 (2021) . https://doi.org/10.3390/en14113191

[7] S. Mashayekh And K. L. Butler-Purry, An Integrated Security-Constrained Model-Based Dynamic Power Management Approach For Isolated Microgrids In All-Electric Ships, In IEEE Trans. Power Syst., 30 (2015) 2934-2945. https://doi.org/10.1109/tpwrs.2014.2377741

[8] Y. Riffonneau, S. Bacha, F. Barruel And S. Ploix, Optimal Power Flow Management For Grid Connected Pv Systems With Batteries, In IEEE Trans. Sustainable Energy, 2 (2011) 309-320. https://doi.org/10.1109/tste.2011.2114901

[9] H. Tazvinga, Z. Bing, and X. Xiaohua, Optimal Power Flow Management for Distributed Energy Resources with Batteries, Energy Convers. Manage., 102 (2015) 104-110. https://doi.org/10.1016/j.enconman.2015.01.015

[10] Z. Yi, W. Dong and A. H. Etemadi, A Unified Control and Power Management Scheme for PV-Battery-Based Hybrid Micro grids for Both Grid-Connected and Islanded Modes, IEEE Trans. Smart Grid, 9 (2018) 5975-5985. https://doi.org/10.1109/tsg.2017.2700332

[11] Q. Jiang, M. Xue And G. Geng, Energy Management Of Microgrid In Grid-Connected And Stand-Alone Modes, IEEE Trans. Power Syst., 28 (2013) 3380-3389. https://doi.org/10.1109/tpwrs.2013.2244104

[12] K. Roy, Optimal Energy Management of Micro Grid Connected System: A Hybrid Approach, Int. J. Energy Res., 45 (2021) 12758-12772. https://doi.org/10.1002/er.6609

[13] P. Harsh, And D. Das, Energy Management In Microgrid Using Incentive-Based Demand Response And Reconfigured Network Considering Uncertainties In Renewable Energy Sources, Sustainable Energy Technol. Assess., 46 (2021). https://doi.org/10.1016/j.seta.2021.101225

[14] S. Kumar, R. K. Saket, P. Sanjeevikumar, & J. B. Holm-Nielsen, A Comprehensive Review On Energy Management In Micro-Grid System, Microgrid Technologies, 2021. https://doi.org/10.1002/9781119710905.ch1

[15] J. J. Joglekar, Power and Energy Management in Micro grid, Micro grid Technologies, Microgrid Technologies, 2021. https://doi.org/10.1002/9781119710905.ch2

[16] M. Kermani, Et Al. Intelligent Energy Management Based on Scada System in a Real Micro grid For Smart Building Applications, Renewable Energy, 171 (2021) 1115-1127. https://doi.org/10.1016/j.renene.2021.03.008

[17] A. Hasankhani, S. M. Hakimi, Stochastic Energy Management of Smart Micro grid With Intermittent Renewable Energy Resources in Electricity Market, Energy, 219 (2021). https://doi.org/10.1016/j.energy.2020.119668

[18] M. A. Hossain, R. K. Chakrabortty, M. J. Ryan, H. R. Pota, Energy Management Of Community Energy Storage In Grid-Connected Microgrid Under Uncertain Real-Time Prices, Sustainable Cities Soc., 66 (2021). https://doi.org/10.1016/j.scs.2020.102658

[19] E. Samadi, A. Badri, And R. Ebrahimpour, Decentralized Multi-Agent Based Energy Management of Micro grid Using Reinforcement Learning, Int. J. Electr. Power Energy Syst., 122 (2020). https://doi.org/10.1016/j.ijepes.2020.106211

[20] C. Schmidt, U. Zimmermann , U. Van Rienen, Modeling Of An Optimized Electrostimulative Hip Revision System Under Consideration Of Uncertainty In The Conductivity Of Bone Tissue, IEEE J. Biomed. Health. Inf., 19 (2015) 1321-1330. https://doi.org/10.1109/jbhi.2015.2423705

[21] H.P.H. Anh, And, C.V. Kien, Optimal Energy Management of Micro grid Using Advanced Multi-Objective Particle Swarm Optimization, Eng. Compute., 37 (2020) 2085-2110. https://doi.org/10.1108/ec-05-2019-0194

[22] , H. J. Kim, M. K. Kim, And J. W. Lee, A Two-Stage Stochastic P-Robust Optimal Energy Trading Management In Micro grid Operation Considering Uncertainty With Hybrid Demand Response, Int. J. Electr. Power Energy Syst., 124 (2021). https://doi.org/10.1016/j.ijepes.2020.106422

[23] S. Fahad, A. J. Mahdi, W. H. Tang, K. Huang and Y. Liu, Particle Swarm Optimization Based Dc-Link Voltage Control For Two Stage Grid Connected Pv Inverter, Int. Conf.Power Syst. Technol., 2018, 2233-2241. https://doi.org/10.1109/powercon.2018.8602128

[24] A. J. Mahdi, S. Fahad, And W. Tang, An Adaptive Current Limiting Controller For A Wireless Power Transmission System Energized By A Pv Generator, Electronics, 9 (2020). https://doi.org/10.3390/electronics9101648

[25] S. Fahad, N. Ullah, A. J. Mahdi, A. Ibeas, A. Goudarzi, An Advanced Two-Stage Grid Connected Pv System: A Fractional-Order Controller, Arxiv Preprint Arxiv: 2004.14106, 2020. https://doi.org/10.48550/arxiv.2004.14106

[26] D. Cardoso Da S., J. S. Dohler, P. M. D. Almeida And J. G. D. Oliveira, Droop Control For Power Sharing And Voltage And Frequency Regulation In Parallel Distributed Generations On Ac Micro grid, 13th IEEE International Conference On Industry Applications (Induscon), 2018, 1-6. https://doi.org/10.1109/induscon.2018.8627328